# Aerosol and dynamical contributions to cloud droplet formation in Arctic low-level clouds

Ghislain Motos[1], Gabriel Freitas[2,3], Paraskevi Georgakaki[1], Jörg Wieder[4,†], Guangyu Li[4], Wenche Aas[5], Chris Lunder[5], Radovan Krejci[2,3], Julie Thérèse Pasquier[4,⊥], Jan Henneberger[4], Robert Oscar David[6], Christoph Ritter[7], Claudia Mohr[2,3,ⁿ], Paul Zieger[2,3], Athanasios Nenes[1,8]

[1]Laboratory of Atmospheric Processes and their Impacts, School of Architecture, Civil & Environmental Engineering, École Polytechnique Fédérale de Lausanne, Lausanne, Switzerland
[2]Department of Environmental Science, Stockholm University, Stockholm, Sweden
[3]Bolin Centre for Climate Research, Stockholm University, Stockholm, Sweden
[4]Department of Environmental Systems Science, Institute for Atmospheric and Climate Science, ETH Zurich, Zurich, Switzerland
[5]NILU—Norwegian Institute for Air Research, Kjeller, Norway
[6]Department of Geosciences, University of Oslo, Oslo, Norway
[7]Alfred Wegener Institute, Helmholtz Centre for Polar and Marine Research, Potsdam, Germany
[8]Center for the Study of Air Quality and Climate Change, Institute of Chemical Engineering Sciences, Foundation for Research and Technology Hellas, Patras, Greece
[†]now at: femtoG AG, Zurich, Switzerland
[⊥]now at: Meteomatics AG, St. Gallen, Switzerland
[ⁿ]now at Laboratory of Atmospheric Chemistry, Paul Scherrer Institute, Villigen, Switzerland

*Correspondence to*: Ghislain Motos (ghislain.motos@epfl.ch), Athanasios Nenes (athanasios.nenes@epfl.ch)

**Abstract.** The Arctic is one of the most rapidly warming regions of the globe. Low-level clouds and fog modify the energy transfer from and to space and play a key role in the observed strong Arctic surface warming, a phenomenon commonly termed "Arctic amplification". The response of low-level clouds to changing aerosol characteristics throughout the year is therefore an important driver of Arctic change that currently lacks sufficient constraints. As such, during the NASCENT campaign (Ny-Ålesund AeroSol Cloud ExperimeNT) extending over a full year from October 2019 to October 2020, microphysical properties of aerosols and clouds were studied at the Zeppelin station (475 m a.s.l.), Ny-Ålesund, Svalbard, Norway. Particle number size distributions obtained from differential mobility particle sizers as well as chemical composition derived from filter samples and an aerosol chemical speciation monitor were analyzed together with meteorological data, in particular vertical wind velocity. The results were used as input to a state-of-the-art cloud droplet formation parameterization to investigate the particle sizes that can activate to cloud droplets, the levels of supersaturation that can develop, the droplet susceptibility to aerosol and the role of vertical velocity. We evaluate the parameterization and the droplet numbers calculated through a droplet closure with in-cloud situ measurements taken during 9 flights over 4 days. A remarkable finding is that, for the clouds sampled in situ, closure is successful in mixed-phase cloud conditions regardless of the cloud glaciation fraction. This suggests that ice production through ice-ice collisions or droplet-shattering may explain have explained the high ice fraction, as opposed to rime-splintering that would have significantly reducereduced the cloud droplet number below levels predicted by warm cloud activation theory. We also show that pristine-like conditions during fall led to clouds that formed over an aerosol-limited regime, with high levels of supersaturation (generally around 1%, although highly variable) that activate particles smaller than 20 nm in diameter. Clouds formed in the same regime in late spring and summer, but

aerosol activation diameters were much larger due to lower cloud supersaturations (c.a. 0.5%) that develop because of higher aerosol concentrations and lower vertical velocities. The contribution of new particle formation to cloud formation was therefore strongly limited, at least until these newly formed particles started growing. However, clouds forming during the Arctic haze period (winter and early spring) can be limited by updraft velocity, although rarely, with supersaturation levels dropping below 0.1% and generally activating larger particles (20 to 200 nm), including pollution transported over a long range. The relationship between updraft velocity and the limiting cloud droplet number agrees with previous observations of various types of clouds worldwide, which ~~confirms~~supports the universality of this relationship.

## 1 Introduction

Greenhouse gas-induced warming is affecting the Arctic more than any other region on the planet (Rantanen et al., 2022). Arctic aerosols have been shown to partially offset local surface warming (Najafi et al., 2015; Breider et al., 2017), which is already impacting the region (Vincent, 2020). Their capacity to form clouds and subsequently impact shortwave and longwave radiation fluxes can strongly influence the regional surface albedo, surface radiation budget, and thus the melting of snow and sea ice (e.g. Curry et al., 1996; Maturilli et al., 2015). Low-level clouds influence the Arctic climate in a substantial but complex manner, with either a positive or a negative forcing depending on the season and the latitude (Intrieri et al., 2002; Shupe and Intrieri, 2004; Tjernström et al., 2014; Tan and Storelvmo, 2019). Arctic low-level clouds are frequently mixed-phase (e.g. Shupe et al., 2008), which makes their representation in models and understanding of their response to cloud condensation nuclei (CCN) availability highly challenging, although critical for understanding Arctic change (e.g., Seinfeld et al., 2016; Sotiropoulou et al., 2016). Extensive long-term observations of aerosols and clouds have been performed in the Arctic (e.g., Platt et al., 2022; Koike et al., 2019); however, aerosol-cloud interactions, and in particular cloud droplet formation processes have to be understood to comprehend the rapid changes occurring in this region of the world. Furthermore, droplet formation and concentrations in mixed-phase clouds (MPCs) are rarely evaluated, even though they can have a profoundly important impact on MPC properties and evolution.

Ny-Ålesund, a scientific settlement based in the Svalbard archipelago, offers a remarkable location for studying the Arctic atmosphere and processes related to aerosol-cloud interactions, with stations located both at sea level and on Zeppelin mountain (475 m a.s.l.). As in the rest of the Arctic, clouds are ubiquitous at Ny-Ålesund, being present 81% of the time (Nomokonova et al.; 2019) with a majority of MPCs, as confirmed by Lawson et al. (2011) over the spring season using a tethered-balloon system. 90% of these MPCs are located below an altitude of 3000 m (Mioche et al., 2015). A combination of ground-based remote sensing observations of cloud properties and the application of broadband radiative transfer simulations allowed us to conclude that clouds have an overall warming effect on the surface at Ny-Ålesund (annual average of 11.1 W m-2), although the net surface cloud radiative effect is negative in summer and positive the rest of the year (Ebell et al., 2020). Ny-Ålesund, owing to both its orographic and maritime landscapes, may also bear atmospheric characteristics that are different from the rest of the Arctic (Maturilli et al., 2019). For example, Mioche et al. (2015) showed that mixed-phase clouds (MPCs) are present around 55% of the time above Ny-Ålesund, whereas in the rest of the Arctic, the mean frequency of occurrence is 30% in the winter and 50%

76   for the rest of the year. Although these statistics can quickly shift owing to the fast warming of the Arctic, they reflect
77   the recent past and give a good indication of the current conditions.

78   Regarding aerosol size distribution, although no site was shown to be representative of the whole Arctic, several
79   features, such as number concentrations and dominant mode of the size distribution throughout the year, are common
80   to Zeppelin and other Arctic sites such as Nord (Greenland), Barrow (Alaska) or Tiksi (Siberia), as shown by Croft et
81   al. (2016) or Freud et al. (2017). Differences to other Arctic stations can be partly related to Zeppelin being located
82   close to the European and American continents, in a sector influenced by warm oceanic currents (Gulf stream) and
83   warm air intrusions, in contrast to other stations surrounded by ice-free ocean. Zeppelin is also often located in the free
84   troposphere (FT; Ström et al., 2009). Nevertheless, a topography analysis suggested that Zeppelin is influenced to a
85   large extent by planetary boundary layer (PBL) air masses (Collaud Coen et al., 2018). Di Liberto et al. (2012) have
86   shown that over a spring day (with no sunset), the station resided in the PBL from 04:00 to 16:00 and in the FT the rest
87   of the day. Such a diurnal cycle is typically observed in lower latitude and higher altitude sites (Collaud Coen et al.,
88   2018).

89   Seasonal patterns of aerosol concentrations and size distributions at the Zeppelin station have been extensively
90   investigated  (e.g. Ström et al., 2003; Tunved et al., 2013; Croft et al., 2016) . The results agree towards a minimum in
91   number concentration at the onset of fall due to efficient cloud scavenging, scarce transport from lower latitudes and
92   limited new particle formation. Concentrations then increase constantly until they reach the spring Arctic haze
93   maximum. The accumulation mode is dominant over this period, until it gets efficiently scavenged in summer, and the
94   Aitken mode then becomes dominant, due to active new particle formation favoured by strong solar radiation and the
95   absence of condensational sinks (Dall´Osto et al., 2017; Park et al., 2021).

96   The seasonality of CCN at Zeppelin tends to follow that of the aerosol particle number concentration (Jung et al., 2018;
97   Koike et al., 2019). Using a counterflow virtual impactor inlet, Karlsson et al. (2021) showed that cloud residuals also
98   follow the same seasonality, but negative temperatures cause cloud residual concentrations to drop compared to aerosol
99   concentration. The dominant Aitken mode in summer does not cause a drop in the number of CCN and cloud residuals,
100  suggesting that also particles down to 20 nm in diameter can activate to cloud droplets during this season (Leaitch et
101  al., 2016; Karlsson et al., 2021). Using aircraft measurements over Alaska, Moore et al. (2011) also showed that most
102  aerosols can act as CCN at supersaturations above 0.1% in this region, i.e. where only particles larger than around 100
103  nm are generally able to activate to cloud droplets. Gramlich et al. (2022) came to the same conclusion by performing
104  chemical analyses of aerosol particles and gases before, during and after cloud, without noting strong variations in
105  chemical composition. CCN are typically associated with accumulation mode particles; however, much smaller
106  particles can activate to cloud droplets if the supersaturations developed in clouds are high enough. Using an adiabatic
107  cloud parcel model, Pöhlker et al. (2021) proposed that in clean environments, such as the Arctic, Aitken mode particles
108  can act as CCN at low updraft velocities (below 1 m s$^{-1}$). Similarly, Bulatovic et al. (2021) reported a strong influence
109  of Aitken mode particles on the subsistence of stratiform Arctic mixed-phase clouds.

110  In the atmosphere, supersaturated air associated with cloudy airmasses leads to the unconstrained condensation of
111  water vapour on CCN, leading to cloud droplet activation. The main mechanism driving this process is expansion
112  cooling of ascending air parcels (e.g. Nenes et al., 2001). Droplet number, however, depends on a combination of the
113  cooling and aerosol forming droplets, either of which can be a "limiting factor", eventually controlling the cloud

susceptibility to aerosol. If the factor limiting droplet formation is the lack of aerosol particles (this is the "aerosol-limited" regime), the droplet concentration is directly proportional to the aerosol number concentration and is effectively independent of updraft velocity. The opposite situation can occur, giving rise to an "updraft-limited" regime (e.g. Jensen and Charlson, 1984; Twomey, 1993) during which cloud droplet formation is insensitive to any further increase in aerosol concentration. Between these two limiting cases, it is expected that a transitional regime also exists, for which cloud droplet formation is sensitive to both updraft velocity and aerosol properties (Reutter et al., 2009). Given the influence of cloud droplet number on cloud radiative effects, knowledge of the prevalent droplet formation regime in various regions of the world and how it varies throughout the year is of primary importance, because it determines the type of optimal constraints (dynamical or aerosol) required in models. Few studies have used this perspective to determine the best observational results for reducing model uncertainties. Regarding the aerosol-CCN-droplet link, several studies focusing on the Arctic have reported that periods of aerosol-limited regime are frequently found (Garrett et al., 2004; Mauritsen et al., 2011; Eirund et al., 2019), but these studies do not cover a whole year, and/or do not fully constrain the aerosol and updraft velocity characteristics and their relation to cloud supersaturation, activated aerosol size, aerosol source/processes and limiting cloud droplet number (i.e., an asymptotic upper limit of droplet number). The Swiss Alps have been the most extensively studied region in that regard so far, using high-altitude ground-based measurements (Hammer et al., 2015; Hoyle et al., 2016; Georgakaki et al., 2021). At other locations, aircraft flights have been used to investigate cloud formation at higher altitudes, e.g., over the United States of America (Bougiatioti et al., 2020) and the southeastern Atlantic ocean (Kacarab et al., 2020).

The Ny-Ålesund AeroSol Cloud ExperimeNT (NASCENT) campaign took place from fall 2019 to fall 2020 over several sites located close to Ny-Ålesund, Svalbard. Pasquier et al. (2022) comprehensively describe the meteorological context, aerosol climatology, instrumental setup as well as first results related to aerosol-cloud interactions (for liquid, ice, and mixed-phase clouds). Here, we utilized in situ data collected during this campaign to feed a cloud droplet formation parameterization in order to unravel the sensitivity of cloud droplet number to aerosol concentration and composition as well as updraft velocity. Sect. 2 describes the NASCENT campaign and the instrumentation used to provide the data for this study. These data serve as input to the cloud droplet parameterization detailed in Sect. 3, where additional analyses linked to specific instruments are also described. In Sect. 4, parameterization outputs are exposed, analyzed and discussed in the broader context of the Arctic seasonal aerosol cycle, together with a droplet closure. Sect. 5 provides concluding remarks.

## 2 Measurements

### 2.1 Measurement site and period

The NASCENT campaign took place in the Svalbard archipelago (also known as Spitsbergen) close to the small seaside settlement of Ny-Ålesund from October 2019 to October 2020. Svalbard itself has very limited anthropogenic aerosol emissions, but it can be influenced by North Atlantic stormy air masses. In order to limit the influence of locally produced sea spray aerosols and make the results more regionally representative, a measurement station located on top of Mount Zeppelin (475 m a.s.l.; 78° 54′ N, 11° 53′ E), approximately two

149 kilometers south of Ny-Ålesund, served as a sampling site for all data presented in this study, unless explicitly stated
150 otherwise.

## 2.2 Instrumentation

### 2.2.1 Particle number size distributions

153 Two differential mobility particle sizers (DMPSs) continuously measured particle number size distribution at the
154 Zeppelin station. In the DMPS, the aerosol is first electrically charged by a 63Ni source, allowing selection by electrical
155 mobility, thus mobility diameter, by a differential mobility analyzer (DMA). Condensation particle counters (CPC,
156 TSI models 3010 for DMPS_1 and 3772 for DMPS_2) then measure the concentration of particles contained in the
157 monodisperse flow. No particle impactor was used. The integration of the particle number size distribution between
158 the boundaries of the measured size spectrum provides the integrated particle number concentration, $N_{aer}$. The DMPSs
159 were connected to a whole-air inlet heated to a temperature of 5-10 °C, following the guidelines of the Global
160 Atmosphere Watch (GAW) program of the World Meteorological Organization (WMO). The size range measured by
161 both DMPSs were 20 to 775 nm for DMPS_1 and 10 to 945 nm for DMPS_2. DMPS_1 and DMPS_2 had a scanning
162 duration of 11 and 7 min, respectively. The size distributions were corrected for particle losses in the inlet using the
163 software tool developed by von der Weiden et al. (2009). More details on the DMPS setup at the Zeppelin station can
164 be found in the study of Karlsson et al. (2021).

### 2.2.2 Aerosol chemical composition

166 The mass concentration of non-refractory bulk aerosol (i.e., species that evaporate rapid at a temperature of 600 °C
167 under vacuum conditions) was measured by a time-of-flight aerosol chemical speciation monitor (ACSM; Fröhlich et
168 al., 2013), whose technology is based on the aerosol mass spectrometer (AMS; Aerodyne Research Inc., Billerica, MA,
169 USA). Measurements were also performed using a 3 stage filter pack system manufactured by the Norwegian Institute
170 for Air Research (NILU) and designed for sampling of particles and gaseous compounds. The filters have a diameter
171 of 47 mm and the flowrate is 12-16 L/min with a sampling duration of 24 hours. First in the direction of the air flow is
172 a Teflon filter (Millipore 3 µm) for collecting ions ($SO_4^{2-}$, $NH_4^+$, $NO_3^-$, $Ca^{2+}$, $K^+$, $Cl^-$, $Na^+$). This is followed by an
173 alkaline (KOH) and an acid (oxalic acid) impregnated filters (Whatman 40) to collect respectively volatile acidic and
174 alkaline components. These instruments sampled behind a whole-air inlet (with a size-cut of around 10 µm, based on
175 tests performed behind the inlet); note however that the ACSM uses a particulate matter larger than 2.5 µm ($PM_{2.5}$)
176 aerodynamic lens. Organic carbon mass concentration was derived from filter samples collected by a Digitel high-
177 volume sampler with a $PM_{10}$ inlet, which operated at a flow rate of 689 L/min over a whole week. The aerosol particles
178 were collected on prefired (850 °C; 3 h) quartz fiber filters (PALLFLEX Tissuequartz 2500QAT-UP; 150 mm in
179 diameter). Thermal-optical analysis (TOA) was performed using a Sunset Lab OC/EC Aerosol Analyzer, using
180 transmission for charring correction, and operated according to the EUSAAR-2 temperature program (Cavalli et al.,
181 2010).
182 Equivalent black carbon (eBC) concentration was retrieved from a multi-angle absorption photometer (MAAP, model
183 5012, Thermo Fisher Scientific, Waltham, MA, USA). This instrument collects particles on a fiber filter and measures

184  the transmission and back scattering of laser light at multiple angles to determine the aerosol absorption coefficient at

185  a wavelength of 637 nm. eBC concentration, calculated from this coefficient using a mass absorption cross-section

186  (MAC) value of 10.6 $m^2$ $g^{-1}$ (as suggested by Ohata et al., 2021), was used to complement both ACSM and filterpack

187  data in order to retrieve aerosol hygroscopicity.

### 2.2.3 Meteorological data

189  Three dimensional wind was continuously observed with a 1 Hz ultrasonic anemometer (model uSonic-3 Omni,

190  METEK GmbH, Elmshorn, SH, Germany), which was placed close to the whole-air inlet. The uSonic measures the

191  speed of sound in between three pairs of transducers and derives a three dimensional (3D) wind vector from the

192  differences of travel path between the three pairs. We inferred updraft velocity from uSonic measurements and could

193  compare it to Doppler wind LiDAR (light detection and ranging) data, which provides 3D profiles starting from around

194  150 m a.g.l. up to 10 km and beyond. The wind LiDAR (WindCube 200, Leosphere, Paris, France; property of

195  AWIPEV) projects a laser beam (vertically for vertical velocity) and measures the Doppler shift between the reference

196  and the backscattered radiation, enabling it to estimate the wind component along the beam propagation direction.

197  Detailed information on the principle of operation as well as recent improvements of the Doppler wind LiDAR can be

198  found in Liu et al. (2019). An overview of the system and the long-term wind pattern over Ny-Ålesund can be found

199  in Graßl et al. (2022). The wind LiDAR was located on the roof of the Atmospheric Observatory of Ny-Ålesund, at an

200  altitude close to sea level and around two kilometers in horizontal distance from Zeppelin (Beck et al., 2017; 2018).

201  A meteorological station located on the roof the Zeppelin station provided data of wind speed and direction,

202  temperature and pressure.

### 2.2.4 Cloud droplet concentration

204  Cloud particle concentrations were sampled with the HOLographic cloud Imager for Microscopic Objects (HOLIMO;

205  Beck et al., 2017; Ramelli et al., 2020) at a height of up to 1000 m above ground for five days in November 2019 and

206  one day in April 2020. HOLIMO can image an ensemble of cloud droplets (with diameter above 6 μm) in a three-

207  dimensional sample volume of about 15 cm³. A convolutional neural network trained and fine-tuned on cloud particles

208  from holographic imagers is used to identify the cloud droplets from artifacts and ice crystals (Touloupas et al., 2020)

209  based on their shape. The smallest detectable ice crystals are 25 μm, and all particles below this threshold are classified

210  as cloud droplets. The holographic imager was attached below the tethered balloon system HoloBalloon (Ramelli et

211  al., 2020; Pasquier et al., 2022). Detailed information about the data taken by the holographic image on the tethered

212  balloon can be found in (Pasquier et al., 2022a).

**3 Data analysis and methods**

**3.1 Particle number size distribution, composition and aerosol hygroscopicity**

Based on the comparison between both DMPSs given in Sect. 4.1, we utilized data from both DMPSs in the analysis of this study, so that gaps in DMPS_1 data are filled with data from DMPS_2. All figures displaying aerosol number concentrations thus include data from both DMPSs.

Organic mass concentration was provided by the ACSM, while organic carbon concentration was measured by a high-volume sampler. The organic carbon concentration given by the filter analysis from this instrument was multiplied by a factor of 2.2 to obtain an estimation of the organic mass concentration, following the recommendations of Turpin and Lim (2001).

Among the species measured by the ACSM, chloride and sodium are assumed to be the only ones predominantly present in the coarse mode. However, the two DMPSs only measured in the submicron range, and the ACSM does not measure sea salt. This is an issue because the inputs of the cloud droplet parameterization should consider the size distribution and hygroscopicity of the same aerosol population. For that reason, chloride and sodium were not included in the calculation of aerosol hygroscopicity. However, we know that these compounds can contribute to the fine mode and increase submicron hygroscopicity at Zeppelin, mostly in winter, as shown by Zieger et al., (2010) and Adachi et al. (2022). To estimate the potential effect of these compounds on our droplet formation results, we performed a sensitivity study, detailed in Sect. 4.3.

Both the ACSM and the filterpack allow for the retrieval of inorganic nitrate, sulphate and ammonium mass concentration. Volume fractions of neutral salts and their hygroscopicity parameters are used as inputs to the volumetric mixing rule required to calculate the total hygroscopicity of the aerosol. For both datasets, we used the simplified ion pairing scheme detailed in Gysel et al. (2007) to calculate the concentration of neutral salts from that of ions, using daily averaged data. From there, the total hygroscopicity parameter κ was introduced by Petters and Kreidenweis (2007) to describe aerosol hygroscopicity based on a semi-empirical parameterization of the Raoult effect. Knowing the hygroscopicity value of each neutral compound - we utilized values listed in Petters and Kreidenweis (2007), Carrico et al. (2010) and Zieger et al. (2017) - the mass-mixing rule enables to estimate the overall aerosol hygroscopicity. We utilized filterpack-derived hygroscopicity values as input to the cloud droplet parameterization described in the next section because the filterpack shows less data gaps than the ACSM over the duration of the NASCENT campaign. ACSM-derived hygroscopicity is thus only used as a validation of the filterpack-derived hygroscopicity values retrieved (see the comparison of both in Fig. S3).

**3.2 Cloud droplet number concentration and cloud supersaturation**

Knowledge of particle number size distribution, overall hygroscopicity parameter κ as well as air temperature and pressure allow for the determination of the potential cloud droplet number concentration, $N_d$, the maximum available cloud supersaturation, $S_{max}$, and the minimum diameter required for an aerosol particle to activate to a cloud droplet, $D_{act}$, using a cloud droplet formation parameterization. Note that the term "potential" is used to describe these outputs because the parameterization results include periods when no clouds were effectively present at Zeppelin. Based on cloud parcel theory, this parameterization was initially developed by Nenes and Seinfeld (2003) and improved with

249     new implementations successively by Fountoukis and Nenes (2005), Barahona et al. (2010) and Morales Betancourt

250     and Nenes (2014). Results of $N_d$ and $S_{max}$ are then constrained by updraft velocity measurements, here given by a

251     uSonic and a wind LiDAR (Sect. 2.2.3). The activation parameterization is based on cloud parcel theory and solves the

252     equations that describe droplet formation in an ascending air parcel containing aerosols and water vapor, specifically

253     at the point where supersaturation becomes equal to $S_{max}$; $N_d$ is then equal to the number of CCN with critical

254     supersaturation less than $S_{max}$. The parameterization uses as inputs the observed pressure and the temperature, the

255     aerosol size distribution data, the hygroscopicity parameter $\kappa$ and the updraft velocities.

256     We extracted wind LiDAR data corresponding to the updraft velocity at 500 m above ground level to make them

257     comparable to uSonic data from Zeppelin station. We noticed surprisingly high values of vertical velocity measured

258     by the uSonic during northern wind conditions (Fig. S1a and S1b), which we attribute to the presence of winds

259     orographically lifted by the Zeppelin mountain. Based on Fig. S1a and S1b, we decided to discard uSonic data when

260     the wind direction was between 335 and 15 degrees, so that any droplet calculation made is more representative of

261     regional conditions than specific conditions at Zeppelin during strong orographically driven updrafts.

262     The high resolution of wind LiDAR and ultrasonic anemometer data reveals the highly variable nature of vertical

263     velocity; to calculate droplet numbers relevant for the average cloud, we use the probabilistic approach detailed in

264     Georgakaki et al. (2021): wind LiDAR data are grouped by hour and each block of 1 hour data is fitted to half-Gaussian

265     probability density functions (PDFs) with a zero mean and a standard deviation $\sigma_w$. The cloud droplet formation

266     parameterization is then applied for a characteristic velocity, $w^* = 0.79\ \sigma_w$, as this provides the average droplet number

267     over the distribution of positive velocities in the domain. A comparison of the results of this analysis derived from the

268     uSonic and the wind LiDAR are shown in Fig. S2. Several studies performed using this approach gave successful

269     droplet closures for $N_d$ and $S_{max}$ in various types of clouds (e.g., Fountoukis et al., 2007; Kacarab et al., 2020;

270     Georgakaki et al., 2021). Note that this approach is not valid for boundary layers that undergo deep convection but

271     only for low vertical velocities typical of boundary layer ascent and descent over a diurnal cycle, which is the case for

272     Zeppelin (Di Liberto et al., 2012; Collaud Coen et al., 2018).

## 273   4 Results and discussion

### 274   4.1 Particle number concentration and size distribution

275     Fig. 1a presents $N_{aer}$ time series, with values that show a minimum in October 2019 (20 - 60 $cm^{-1}$) followed by a

276     relatively constant increase until an upper plateau (100 - 1000 $cm^{-1}$) reached between May and August 2020. A sharp

277     decrease in $N_{aer}$ is then observed towards the October minimum. These measurements are in good agreement with the

278     annual cycle of integrated particle concentration at Zeppelin reported by Tunved et al. (2013), who measured particle

279     number size distribution between 20 and 630 nm before 2005 and between 10 and 790 nm after, and averaged the

280     results over ten years from 2000 to 2010. However, we note a one-month lag in the appearance of the high concentration

281     plateau (reported from April to July, whereas it appears from the beginning of May to the end of August in the present

282     study). Aerosol levels measured at Zeppelin during the NASCENT campaign can thus be considered typical for this

283  site. Overlapping periods of both DMPSs allow for a comparison of $N_{aer}$ (see Fig. 1b) and confirm the strong correlation
284  between both instruments.

285
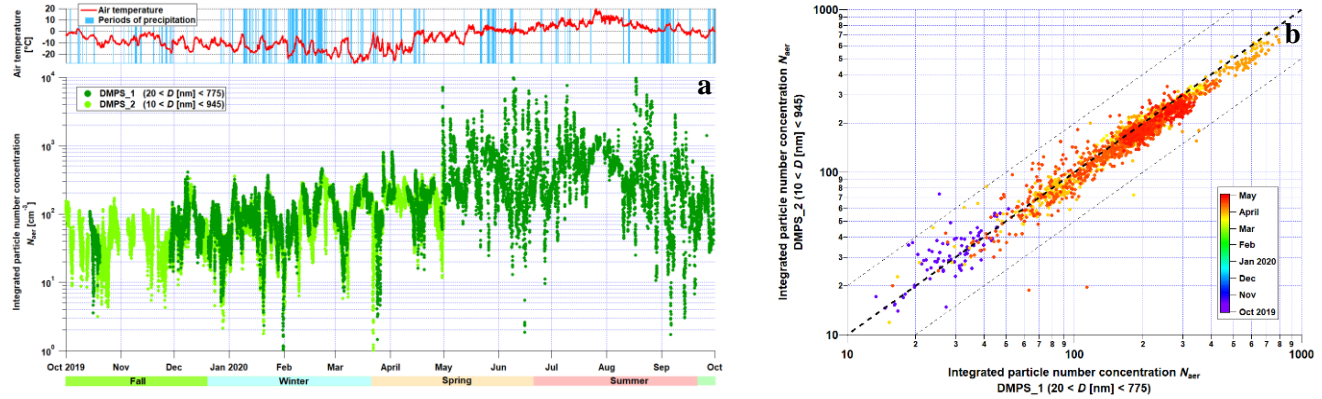


286
287  **Figure 1. a): Air temperature measured by a probe (top panel) and integrated particle number concentration $N_{aer}$ (bottom**
288  **panel) as measured by two DMPS systems at the Zeppelin station, displayed as time series. It should be noted that the two**
289  **DMPSs have different size ranges: 20 to 775 nm for DMPS_1; 10 to 945 nm for DMPS_2. b): Comparison of integrated**
290  **particle number concentration $N_{aer}$ as measured by two differential mobility particle sizer (DMPS) systems at Zeppelin, with**
291  **the date as colour scale.**

292  **4.2 Aerosol hygroscopicity parameter κ**

293  The time series of κ values derived from both the filterpack and the ACSM data is shown in Fig. S3a. Both instruments,
294  despite being based on techniques with a different aerosol size cut-off (PM$_{2.5}$ for the ACSM and PM$_{10}$ for the
295  filterpack), generally provide κ values that agree to within 50% for the majority of data points (Fig. S3b). The mean
296  hygroscopicity parameter κ value over the whole campaign was 0.40 when derived from the ACSM and 0.32 from the
297  filterpack. Temporal trend shows a relatively constant κ value around 0.3 in fall, winter and spring, but a slightly lower
298  value in summer, dropping to approximately 0.2, although rather variable.

299       A small number of field campaigns at Zeppelin investigated aerosol hygroscopicity. In summer 2008, Zábori
300  et al., (2015) utilized both bulk chemical composition and size-resolved CCN measurements, retrieving κ values of
301  respectively 0.5 and 0.3-0.4, slightly higher than our results. Zieger et al. (2010) measured wet and dry aerosol
302  scattering from July to October 2008 using humidified and dry nephelometers. Using Mie theory, they were able to
303  retrieve the hygroscopicity parameter κ and found a mean value of 0.57. This is also higher than the values we report
304  in Fig. S3a, but the techniques used and the seasons studied are different. The median κ value of 0.23, retrieved by
305  Jung et al. (2018), based on 5 years of CCN-scanning mobility particle sizer (SMPS) measurements, however agree
306  with our results. Year-round hygroscopic growth measurements by Rastak et al., (2014) led to the conclusion that the
307  influence of hygroscopic growth on the direct radiative effect was higher in summer than during the Arctic Haze period.
308  The hygroscopicity parameter has been constrained also in other locations in the Arctic, all of them combining a CCN
309  counter and an instrument measuring particle number size distribution, either an ultra-high sensitivity aerosol
310  spectrometer (UHSAS), a SMPS or a DMPS to provide input data for κ-Köhler theory calculations. Moore et al. (2011)
311  and Herenz et al. (2018) both characterized springtime Arctic aerosol. The former reported values around 0.4 for
312  background air masses and slightly below 0.6 for Arctic boundary layer in aircrafts flying over northern Alaska (USA);

9

313   the latter retrieved a κ value of 0.23 at a station located in the Inuvik region in Canada. Martin et al. (2011) and Lathem

314   et al. (2013) ran measurements in the summer season and found similar values (average of 0.33 and 0.32, respectively),

315   on an icebreaker on its way from Svalbard to the proximity of the North pole and on aircrafts flights between Alberta

316   (Canada) and Greenland. Also in summer, but at a ground-based station in northern Sweden (68° North), Kammermann

317   et al. (2010) retrieved lower κ values, between 0.07 and 0.21, but the close presence of the Stordalen mire, known to

318   emit organic precursors, could cause a local reduction in aerosol hygroscopicity. At the Villum station in northeastern

319   Greenland, Massling et al. (2022) reported κ values very close to the present study using CCN-SMPS measurements:

320   0.28-035 in spring, and 0.23-0.35 in summer.

### 4.3 Potential cloud supersaturation, droplet number concentration and activation diameter

322   The cloud droplet formation parameterization outputs $S_{max}$, $N_d$ and $D_{act}$ are displayed as frequency of occurrence in Fig.

323   2 and as a time series in Fig. S4 with the measured values of $\sigma_w$, which are used to constrain the parameterization.

324   During periods of rain (noted in Fig. 1a), the aerosol load was strongly reduced, directly implying sharp decreases in

325   $N_d$ and $D_{act}$ which impact the other parameters. As expected, $S_{max}$ and $\sigma_w$ covaried during the whole year, since

326   turbulence and vertical velocity are primary drivers of cloud supersaturation generation. Values of $S_{max}$ were highest

327   in fall, centered around 1% and reaching up to 4% (Fig. 1b). Except for a drop in early August, $S_{max}$ values ranged

328   between around 0.5% and 1.5% in the second half of spring and in summer.

329   Together with Bougiatioti et al. (2020), Kacarab et al. (2020) examined the conditions for which cloud formation is

330   insensitive to any increase in $N_{aer}$ (i.e., updraft-limited regime) and found that it corresponds to when $S_{max}$ is below

331   0.1%. Subsequent studies (e.g., Georgakaki et al., 2021) also supported this criterion, which is the one we decided to

332   use here as well. Fig. S4b indicates that such conditions only occurred over short periods in winter and during the first

333   half of spring. This shows that updraft velocity-limited conditions can be found, although very rarely, in the Svalbard

334   archipelago when aerosol concentrations approach the Arctic haze maximum in winter and early spring (Fig. 2a and

335   S4b). This is an important result, because when these conditions occur, cloud formation is not linearly influenced by

336   these large aerosol loads, but only until a certain threshold, which will be discussed in the following. The presence of

337   very large particles, larger than the maximum diameter that can be detected by the DMPSs, could potentially scavenge

338   water vapour and cause drops in $S_{max}$, as low as those we observed. However, the mode diameter measured during the

339   campaign was consistently between about 30 and 300 nm, and particles larger than 500 nm were very rare (not shown),

340   in agreement with previous literature at the same site (Tunved et al., 2013; Pasquier et al., 2022b). We thus consider it

341   very unlikely that low values of Smax are caused by this phenomenon.

342   $N_d$, however, is not clearly linked to $S_{max}$, but follows the trend of $N_{aer}$ shown in Fig. 1a (this is confirmed by the

343   scatterplots in Fig. 3) because a higher number of aerosol particles goes with a higher number of CCN on which water

344   vapour can condense, as shown at Zeppelin by Jung et al. (2018). On the other hand, higher $N_{aer}$ also results in a more

345   intense competition for water vapour, leading to a decrease in $S_{max}$, which in turn tends to limit $N_d$. Measuring the

346   annual cycle of cloud residual number concentration at the same site from November 2015 to February 2018 using a

347   ground-based counterflow virtual impactor (GCVI) inlet, Karlsson et al. (2021) reported a similarly high and variable

348   plateau between April and August as well as a minimum in fall. They however reported very low concentrations in

January in February, followed by ~~an extremely~~ a very sharp increase from March to April. Our results show a steadier increase over the whole winter, in agreement with the increase in $N_{aer}$ (Fig. 1a).

Clear seasonal variations in $D_{act}$ can also be seen: the pristine-like conditions in fall and early winter associated with high cloud supersaturations led to low values of $D_{act}$, with frequent occurrences below 20 nm (Fig. 2c and S4d). These are even lower diameters than the values reported by Koike et al. (2019) – minimum $D_{act}$ around 30 to 50 nm – using air parcel model calculations. Together with relatively high $S_{max}$ at this period of the year, the very low aerosol concentrations, mainly concentrated in the accumulation mode (Tunved et al., 2013), leads to their efficient activation to cloud droplets, in agreement with previous results from Siegel et al. (2022). Although anthropogenic pollution transported from lower latitudes during the Arctic haze period (late winter and spring; Rahn, 1981; Hirdman et al., 2010) controls the CCN and droplet population, only a fraction of it was activated to cloud droplets, as larger $D_{act}$ values, centered around 50-100 nm, were in the range of accumulation mode particles typically linked to this type of atmospheric transport. Such $D_{act}$ values persisted over the summer with a particularly high peak between 100 and 200 nm at the beginning of August. Similarly, the dominant Aitken mode, originating from the intense new particle formation activity, likely stayed to a very large extent in the interstitial (unactivated) phase.

The comparison between uSonic- and wind LiDAR-derived updraft velocity shown in Figure S1 and S2 provides relatively accurate but not very precise results, which could be due to fine-scale variability in vertical motion but also to larger-scale differences related to the horizontal distance between both instruments. However, Fig. 2 and S4 provide a good indication of the second order influence of the updraft velocity on the outputs of the cloud droplet formation parameterization, since the $N_d$, $S_{max}$ and $D_{act}$ results based on the wind LiDAR and on the uSonic strongly agree.

With a view to consistency with data from the DMPSs, the cloud droplet parameterization outputs shown in Fig. 2 and S4 are based on hygroscopicity calculations that do not include sodium and chloride, under the assumption that submicron aerosol particles do not contain these compounds. According to Adachi et al. (2022), this assumption may not be fully correct, as particles of 1 μm in winter are found to be composed of 50% by mass of sea salt, with a decreasing proportion with decreasing particle diameter. To address any effects of sea salt on droplet formation, we performed a sensitivity analysis assuming the extreme case for which half of the measured aerosol mass was sea salt and repeated the analysis detailed above. Using a κ value of 1.1 for sea salt, as suggested by Zieger et al. (2017), the overall hygroscopicity shifted from values of 0.2-0.3 (see Fig. S3) to around 0.7. Fig. S5 shows the seasonal percent change such an increase in aerosol hygroscopicity has on $N_d$, $S_{max}$ and $D_{act}$. The two former parameters are very slightly affected in fall, winter and spring (up to ~5% for $N_d$). In summer they undergo a 20% change, but this is the season when the effective sea salt fraction is the lowest, as shown by Adachi et al. (2022), making such an effective change particularly unlikely. Values of $D_{act}$ are more affected, although moderately with a reduction of around 30% regardless of the season. Overall, this sensitivity analysis shows that aerosol hygroscopicity effects from sea salt may have a second order influence on the cloud droplet parameterization outputs, and thus, would not significantly affect the results and conclusions based on the base case hygroscopicity value.

384



385

12
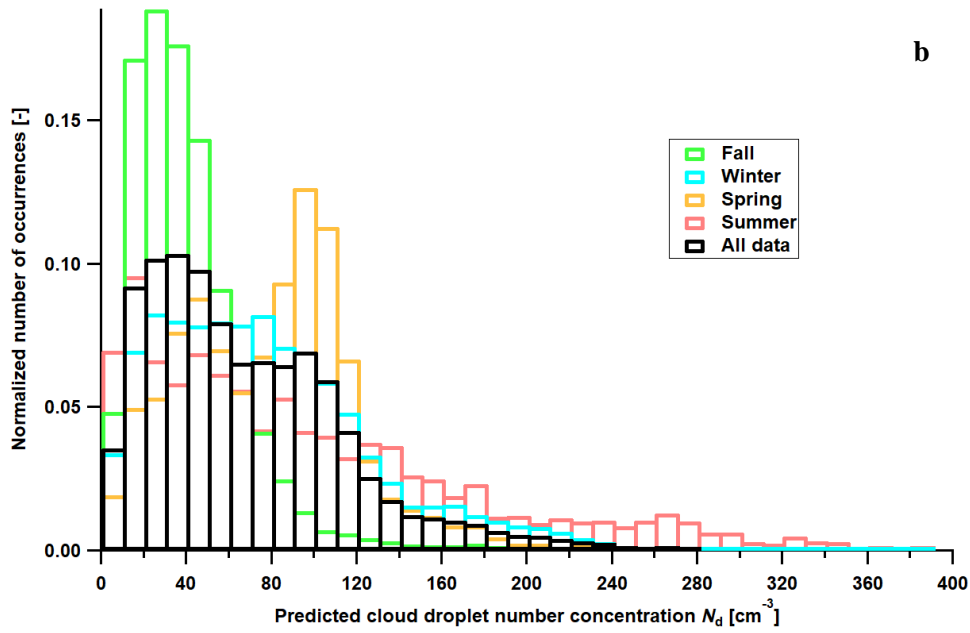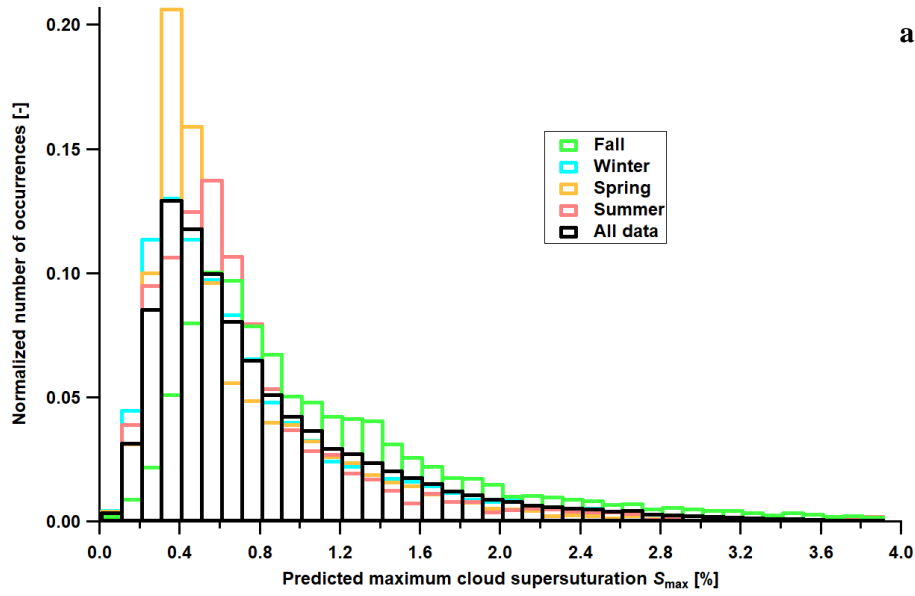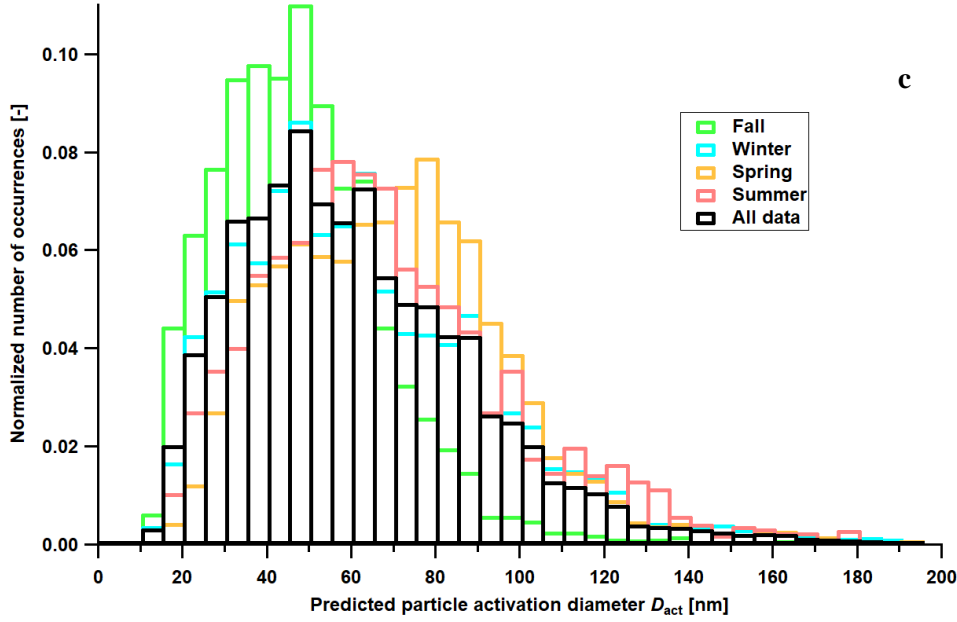
**Figure 2. Normalized number of occurrences of a) $S_{max}$, b) $N_d$ and c) $D_{act}$ during the NASCENT campaign. The data is divided per season: fall (green), winter (light blue), spring (orange) and summer (red).**

### 4.4 Limiting droplet number concentration

During updraft-limited cloud formation conditions, values of $N_d$ reach an upper limit, independent on $N_{aer}$, which Kacarab et al. (2020) suggested to name the limiting droplet number concentration, $N_d^{lim}$. This upper limit can be visualized as a plateau for which $S_{max}$ drops below 0.1% when plotting $N_d$ as a function of $N_{aer}$. This is shown in Fig. 3, where as a sensitivity analysis, we prescribed three different $\sigma_w$ values, 0.1, 0.2 and 0.3 m s$^{-1}$ for running the cloud droplet parameterization. Note that the three values of $\sigma_w$ chosen here are representative of the stratiform cloud conditions typically prevailing in the Arctic (Shupe et al., 2008b). Based on the results in Sect. 4.3, updraft-limited conditions were observed in winter and early spring. Extracting mean plateau values corresponding to these seasons from Fig. 3, we retrieved $N_d^{lim}$ values of 173 cm$^{-3}$ for winter and 128 cm$^{-3}$ for spring, when an updraft velocity $\sigma_w = 0.1$ m s$^{-1}$ is prescribed. These results are in good agreement with the 2 years averaged peak concentration of cloud residuals measured by Karlsson et al. (2021) for April and May. This implies that when updraft velocity was low at the Zeppelin station in winter and early spring, only the fraction of the aerosol number concentration corresponding to these seasonal plateau values formed cloud droplets; any surplus of aerosol (very likely during Arctic haze conditions) remained in the interstitial phase.

Adding up to the different regimes of cloud formation distinguished in Sect 4.3., the $N_d^{lim}$ plateau is almost never reached in fall and in summer. Short drops in $S_{max}$ below 0.1% occurred, e.g. at the beginning of December and August as shown in Fig. 1b, but over too short periods for them to be associated as updraft velocity-limited conditions. For that reason, we do not consider the summer $S_{max}$ values below 0.1% in Fig. 3 as a relevant $N_d^{lim}$ plateau value.

In addition, it is worth noting that when applying the same analysis with an assumption on $\sigma_w$ larger than 0.1 m s$^{-1}$ (i.e., 0.2 or 0.3 m s$^{-1}$); middle and right panels in Fig. 3) and even higher (not shown), the 0.1% $S_{max}$ threshold is not reached

13

409    at all, neither in winter nor in spring, indicating that vertical velocity-limited conditions cannot be found if the

410    turbulence of the boundary layer is not extremely low.

411    Observing the shape of the plots displayed in Fig. 3 also provides information on the efficiency of cloud droplet

412    formation and corroborates the results discussed above. The high $S_{max}$ and corresponding low $D_{act}$ in fall and winter

413    are associated to the droplet activation of the whole aerosol population, leading $N_d^{lim}$ to match $N_{aer}$; these two

414    parameters are thus represented in a scatterplot as a narrow band close to the 1:1 relationship. On the contrary, the

415    scatterplot for the summer season shows a much larger spread with an offset from the 1:1 line, in agreement with a

416    large proportion of Aitken mode aerosol particles that did not activate to cloud droplets. Interestingly, the sharp

417    transition between these two activation behaviours, also observed by Engvall et al. (2008) and which we have shown

418    to occur in the middle of spring(Fig. 2a-b-c and S4b-c-d), results in a scatterplot where both staggered and matching

419    $N_d$ - $N_{aer}$ relationships can be observed.

420    Extracting the plateau values of $N_d^{lim}$ from Fig. 3, we investigate their relationship with $\sigma_w$ in different types of clouds

421    located in various geographic locations using previous studies in which the same probabilistic analysis was performed

422    (Fig. 4). Kacarab et al. (2020) measured from an aircraft in summer in the marine boundary layer over the southeastern

423    Atlantic, a region that can be strongly influenced by biomass burning fires from the African continent. They retrieved

424    values of $\sigma_w$ between 0.30 (relatively clean air mass) and 0.56 m s$^{-1}$ (more polluted) for which $N_d^{lim}$ was reached.

425    Georgakaki et al. (2021) also reported $\sigma_w$ values as high as 0.5 m s$^{-1}$ in two mid-altitude stations located in the Swiss

426    Alps in central Europe. The fact that they had winter measurements allowed them to reach values as low as 0.1 m s$^{-1}$,

427    making their results directly comparable to those shown here. They could link this value of $\sigma_w$ to an $N_d^{lim}$ plateau of

428    108.1 cm$^{-3}$. At the other side of the spectrum, Bougiatioti et al. (2020) reached an $N_d^{lim}$ plateau for $\sigma_w$ values as high

429    1.2 m s$^{-1}$ thanks to late spring and summer flights in the boundary layer over the southeastern United States. They

430    proposed the following linear correlation between $N_d^{lim}$ [cm$^{-3}$] and $\sigma_w$ [m s$^{-1}$]: $N_d^{lim}$ = 1033.9 $\sigma_w$ + 112.28 (R2 = 0.92).

431    Georgakaki et al. (2021) updated this relationship, including the results from Kacarab et al. (2020) and their own: $N_d^{lim}$

432    = 1137.9 $\sigma_w$ – 17.1, and proved very strong agreement between all reported data ($R^2$ = 0.94). The two additions from

433    the present study, associated to winter and spring plateau values for $\sigma_w$ = 0.1 m s$^{-1}$, also agree well with these previous

434    results, although they were retrieved in a very different environment, relatively clean with clouds mainly originating

435    from maritime air masses and uplifted in mountainous terrain. This provides another confirmation of the robustness of

436    the empirically demonstrated $\sigma_w$ - $N_d^{lim}$ relationship regardless of the environment, type of clouds and aerosol sources.
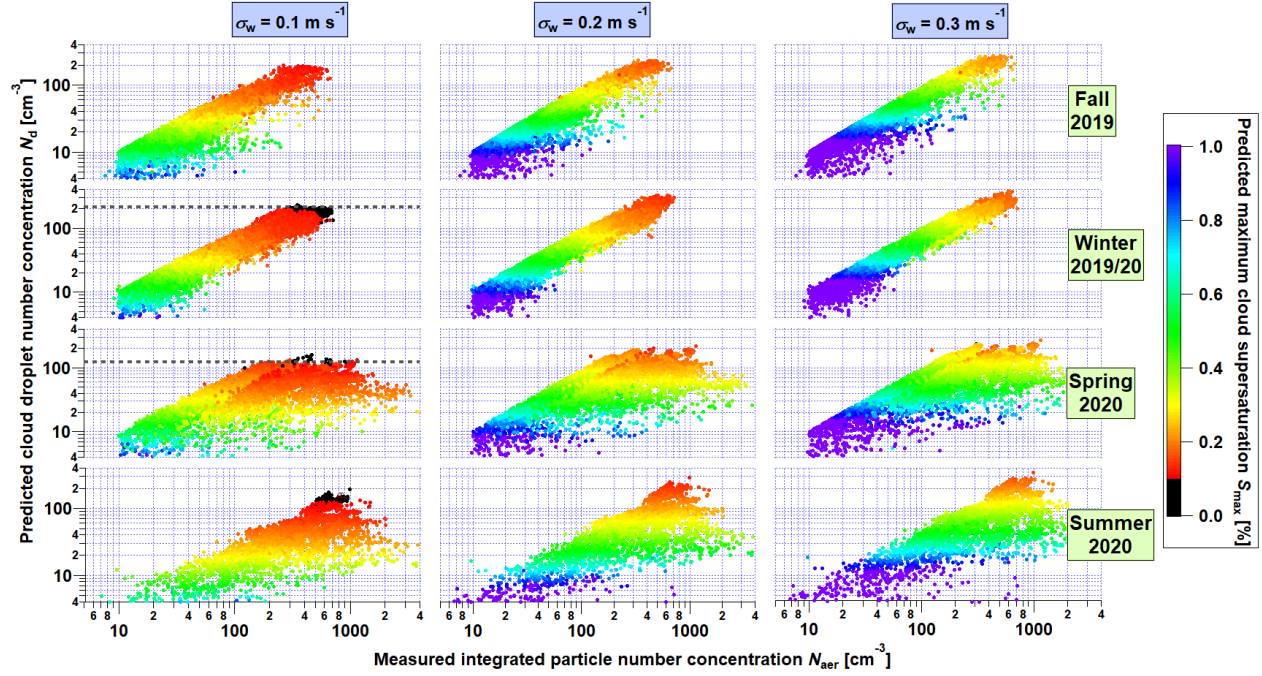
**Figure 3. Predicted potential droplet number concentration $N_d$ compared to integrated particle number concentration $N_{aer}$. Data are shown in 12 panels corresponding to four seasons and three different assumptions on updraft velocity $\sigma_w$: 0.1, 0.2 and 0.3 m s⁻¹. $N_d$ is an output of the cloud droplet formation parameterization and $N_{aer}$ is measured by the DMPSs. The colour scale is the maximum predicted cloud supersaturation $S_{max}$; note that data points for which $S_{max} <0.1\%$ are shown in black. Plateau values of $N_d^{lim}$, calculated as the average value of data points for which $S_{max} <0.1\%$, are displayed as grey dotted lines.**
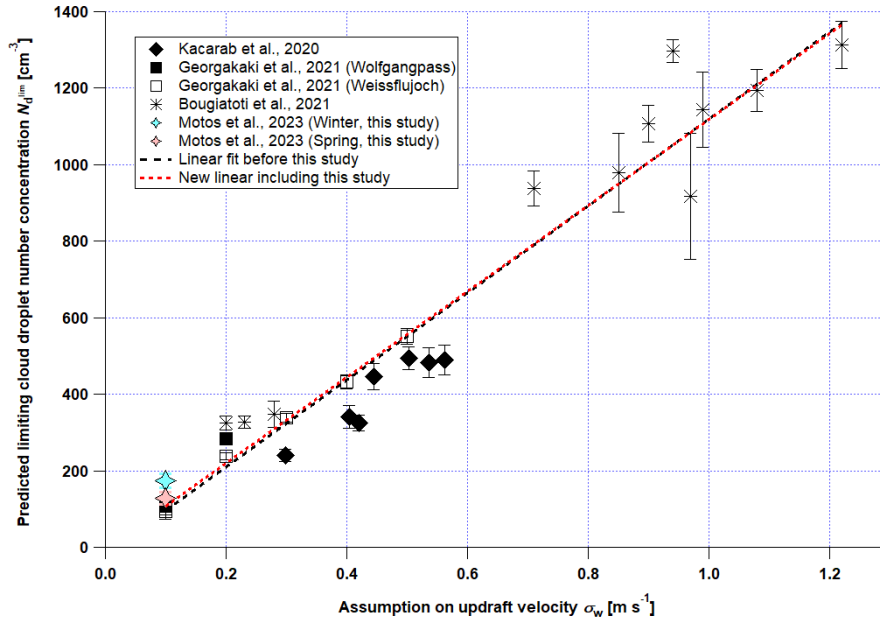


**Figure 4. Predicted limiting cloud droplet number concentration plotted against the corresponding assumption on the updraft velocity, comparing the present study with existing literature. The linear fit displayed in black is the one given by Georgakaki et al. (2021); the red one includes results from the current study.**

15

## 4.5 Droplet closure

$N_d$ is one of the outputs provided by the cloud droplet formation parameterization utilized in the present study (see Fig. 2b and S4c). The availability of instruments measuring this parameter facilitates the validation of the cloud droplet parameterization by comparing in situ data with the parameterization output. This was achieved several times in past studies through successful droplet closures (e.g. Fountoukis et al., 2007; Kacarab et al., 2020), and can also be performed here using measurements from the HOLIMO taken on 9 HoloBalloon flights during the NASCENT campaign (Fig. 5; see Pasquier et al. (2022a) for detailed descriptions of the atmospheric conditions during the flights. We note that, based on the radar measurements they performed, the clouds studied in November 10, 11 and 12, 2019 were monolayer clouds, but the April 1st case is a typical seeder-feeder configuration, with a synoptic cloud above the sampled cloud). The closure, which is assessed to be attained when predictions were within a factor 2 of observations, appears successful for $N_d > 8$-$10$ cm$^{-3}$, thereby validating the use of the cloud droplet formation parameterization in the Arctic environment. Values of $N_d$ below 8-10 cm$^{-3}$ approach the minimum threshold concentration for which a cloud can still be defined as such, potentially including periods when droplet nucleation is not effectively occurring or has been followed by out-of-cloud scavenging.

Mixed-phase clouds tend to rapidly glaciate (i.e., convert to pure ice clouds) due to the Wegener-Bergeron-Findeisen (WBF) process or riming (Korolev et al., 2017), which can effectively transfer mass from the liquid to the ice phase. Nevertheless, Fig. 5 provides evidence that even for a degree of glaciation (i.e., the fraction of cloud water that is in the form of ice) as high as 90%, cloud parcel activation theory can predict $N_d$ to within 50% of observations. This implies that significant amounts of glaciation over the duration of the HoloBalloon flights, and possibly over spring and fall may have occurred through processes that do not deplete droplet number, e.g. WBF that is promoted by secondary ice production (SIP) through ice-ice collisions or droplet-shattering (Field et al., 2017; Korolev and Leisner, 2020). SIP through rime-splintering is unlikely as it would have reduced the available $N_d$. This hypothesis is in line with the findings of Pasquier et al. (2022a), where the effect of SIP was inferred in about 40% of the in-cloud measurements.

Previous observations (Borys et al., 2003; Lance et al., 2011; Norgren et al., 2018) reported that large aerosol loadings could hamper the efficiency of riming in mixed-phase clouds. Here we show that even in the very pristine conditions during winter and spring, the amount of riming does not seem to affect the droplet number concentrations significantly from what is expected from warm cloud activation theory.
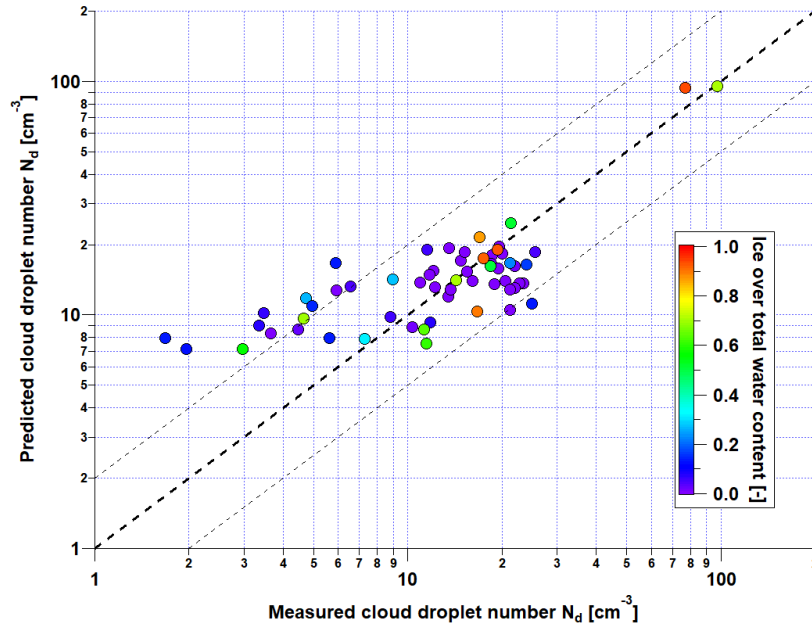
Figure 5. Scatterplot of predicted against measured cloud droplet number $N_d$ during 9 HoloBalloon flights on November 10, 11, 12 2019 and April 1st, 2020.

## 5 Summary and Conclusions

Measurements performed over a whole year at the Zeppelin station in the Svalbard archipelago, in the framework of the NASCENT campaign, served as inputs for a semi-empirical parameterization whose use was validated through a droplet closure. This led to unravel different characteristics of cloud droplet formation in the Arctic environment:

• Several recently published studies focusing on the factors limiting cloud droplet formation were able to distinguish periods of aerosol-limited or updraft velocity-limited cloud droplet formation regimes in boundary layer clouds with high updraft velocities such as cumulus and stratocumulus clouds, but also in alpine mixed-phase clouds that can form in more stable air dynamics. The current study demonstrates that updraft-velocity cloud formation can also occur in a relatively unpolluted environment with weak convection of maritime air masses such as the Arctic, during winter and early spring.

• During the fall and early winter period, the high cloud supersaturations encountered allow to efficiently activate to cloud droplets the vast majority of the aerosol population. By late winter and spring (Arctic Haze period), accumulation mode particles transported over long-range pathways contribute to cloud formation, although cloud supersaturations, and hence activation diameters, are highly variable. Interestingly, the onset of intense new particle formation in summer coincides with an increase in activation diameters. Newly formed and dominant Aitken mode particles thus barely participate in cloud formation before they grow to larger sizes over the course of summer and fall.

• The recent interest in understanding the response of the limiting droplet number concentration to variations in updraft velocity has led to describe a relationship between these two parameters that showed to be strikingly similar in very diverse environments, intensities of atmospheric convection and types of clouds. We showed that, as unpolluted and weakly dynamic as it is, the Arctic environment is no exception. This is an important step towards the confirmation of the universality of the $N_d^{\mathrm{lim}}$ - $\sigma_w$ relationship.

17

500  • Insights into the mechanisms of secondary ice production in the Arctic spring and fall could be extracted from our
501  droplet closure. Although the measurements were taken over 4 days only and may not be representative of the whole
502  year, they suggest that riming was not taking place in any significant amount, leaving room for ice-ice collisions and
503  droplet shattering (alongside with WBF) as the main mechanisms of glaciation, in addition to primary ice production.
504  This also ~~means~~argues that warm cloud activation theory, such as described by well-established activation
505  parameterizations (e.g., Morales and Nenes, 2014) are appropriate for application in mixed-phase cloud simulations.

## Data availability

507  All datasets are available upon request from the contact author.

## Author contribution

509  GM and AN conceived and designed the study. GM, AN and PG developed the data analysis methods, AN developed
510  the droplet calculation codes and performed the simulations with GM. GM authored the manuscript with input from
511  AN and PG. CR provided the wind lidar data. CL and WA provided the chemical composition data (filterpack and
512  ACSM) from Zeppelin. JW helped with ground-based aerosol and the balloon-borne cloud measurements, and
513  contributed to the discussion and interpretation. ROD helped with the balloon-borne and conducted the mountaintop
514  cloud measurements. All co-authors commented on the manuscript and provided feedback. RK, PZ and GF provided
515  aerosol microphysical and meteorological data from Zeppelin station and contributed to the interpretation and
516  manuscript editing and commenting.

## Competing interests

518  The authors declare that they have no conflict of interest.

530 and ACSM measurements are provided by the Norwegian Ministry of Climate and Environment while the inorganic

531 measurements from the filterpack are funded by the Norwegian Environment Agency.


532 **References**

533 Adachi, K., Tobo, Y., Koike, M., Freitas, G., Zieger, P., and Krejci, R.: Composition and mixing state of Arctic aerosol

534 and cloud residual particles from long-term single-particle observations at Zeppelin Observatory, Svalbard,

535 Atmospheric Chemistry and Physics, 22, 14421–14439, https://doi.org/10.5194/acp-22-14421-2022, 2022.


536 Barahona, D., West, R. E. L., Stier, P., Romakkaniemi, S., Kokkola, H., and Nenes, A.: Comprehensively accounting

537 for the effect of giant CCN in cloud activation parameterizations, Atmospheric Chemistry and Physics, 10, 2467–2473,

538 https://doi.org/10.5194/acp-10-2467-2010, 2010.


539 Beck, A., Henneberger, J., Schöpfer, S., Fugal, J., and Lohmann, U.: HoloGondel: in situ cloud observations on a cable

540 car in the Swiss Alps using a holographic imager, Atmospheric Measurement Techniques, 10, 459–476,

541 https://doi.org/10.5194/amt-10-459-2017, 2017.


542 Beck, A., Henneberger, J., Fugal, J. P., David, R. O., Lacher, L., and Lohmann, U.: Impact of surface and near-surface

543 processes on ice crystal concentrations measured at mountain-top research stations, Atmospheric Chemistry and

544 Physics, 18, 8909–8927, https://doi.org/10.5194/acp-18-8909-2018, 2018.


545 Borys, R. D., Lowenthal, D. H., Cohn, S. A., and Brown, W. O. J.: Mountaintop and radar measurements of

546 anthropogenic aerosol effects on snow growth and snowfall rate, Geophysical Research Letters, 30,

547 https://doi.org/10.1029/2002GL016855, 2003.


548 Bougiatioti, A., Nenes, A., Lin, J. J., Brock, C. A., de Gouw, J. A., Liao, J., Middlebrook, A. M., and Welti, A.: Drivers

549 of cloud droplet number variability in the summertime in the southeastern United States, Atmospheric Chemistry and

550 Physics, 20, 12163–12176, https://doi.org/10.5194/acp-20-12163-2020, 2020.


551 Breider, T. J., Mickley, L. J., Jacob, D. J., Ge, C., Wang, J., Payer Sulprizio, M., Croft, B., Ridley, D. A., McConnell,

552 J. R., Sharma, S., Husain, L., Dutkiewicz, V. A., Eleftheriadis, K., Skov, H., and Hopke, P. K.: Multidecadal trends in

553 aerosol radiative forcing over the Arctic: Contribution of changes in anthropogenic aerosol to Arctic warming since

554 1980, Journal of Geophysical Research: Atmospheres, 122, 3573–3594, https://doi.org/10.1002/2016JD025321, 2017.


555 Bulatovic, I., Igel, A. L., Leck, C., Heintzenberg, J., Riipinen, I., and Ekman, A. M. L.: The importance of Aitken mode

556 aerosol particles for cloud sustenance in the summertime high Arctic – a simulation study supported by observational

557 data, Atmospheric Chemistry and Physics, 21, 3871–3897, https://doi.org/10.5194/acp-21-3871-2021, 2021.

558 Carrico, C. M., Petters, M. D., Kreidenweis, S. M., Sullivan, A. P., McMeeking, G. R., Levin, E. J. T., Engling, G.,

559 Malm, W. C., and Collett, J. L. J.: Water uptake and chemical composition of fresh aerosols generated in open burning

560 of biomass, Atmospheric Chemistry and Physics, 10, 5165–5178, https://doi.org/10.5194/acp-10-5165-2010, 2010.

561 Cavalli, F., Viana, M., Yttri, K. E., Genberg, J., and Putaud, J.-P.: Toward a standardised thermal-optical protocol for

562 measuring atmospheric organic and elemental carbon: the EUSAAR protocol, Atmospheric Measurement Techniques,

563 3, 79–89, https://doi.org/10.5194/amt-3-79-2010, 2010.

564 Collaud Coen, M., Andrews, E., Aliaga, D., Andrade, M., Angelov, H., Bukowiecki, N., Ealo, M., Fialho, P., Flentje,

565 H., Hallar, A. G., Hooda, R., Kalapov, I., Krejci, R., Lin, N.-H., Marinoni, A., Ming, J., Nguyen, N. A., Pandolfi, M.,

566 Pont, V., Ries, L., Rodríguez, S., Schauer, G., Sellegri, K., Sharma, S., Sun, J., Tunved, P., Velasquez, P., and Ruffieux,

567 D.: Identification of topographic features influencing aerosol observations at high altitude stations, Atmospheric

568 Chemistry and Physics, 18, 12289–12313, https://doi.org/10.5194/acp-18-12289-2018, 2018.

569 Croft, B., Martin, R. V., Leaitch, W. R., Tunved, P., Breider, T. J., D'Andrea, S. D., and Pierce, J. R.: Processes

570 controlling the annual cycle of Arctic aerosol number and size distributions, Atmospheric Chemistry and Physics, 16,

571 3665–3682, https://doi.org/10.5194/acp-16-3665-2016, 2016.

572 Curry, J. A., Schramm, J. L., Rossow, W. B., and Randall, D.: Overview of Arctic Cloud and Radiation Characteristics,

573 Journal of Climate, 9, 1731–1764, https://doi.org/10.1175/1520-0442(1996)009<1731:OOACAR>2.0.CO;2, 1996.

574 Dall´Osto, M., Beddows, D. C. S., Tunved, P., Krejci, R., Ström, J., Hansson, H.-C., Yoon, Y. J., Park, K.-T., Becagli,

575 S., Udisti, R., Onasch, T., O´Dowd, C. D., Simó, R., and Harrison, R. M.: Arctic sea ice melt leads to atmospheric new

576 particle formation, Sci Rep, 7, 3318, https://doi.org/10.1038/s41598-017-03328-1, 2017.

577 Di Liberto, L., Angelini, F., Pietroni, I., Cairo, F., Di Donfrancesco, G., Viola, A., Argentini, S., Fierli, F., Gobbi, G.,

578 Maturilli, M., Neuber, R., and Snels, M.: Estimate of the Arctic Convective Boundary Layer Height from Lidar

579 Observations: A Case Study, Advances in Meteorology, 2012, e851927, https://doi.org/10.1155/2012/851927, 2012.

580 Ebell, K., Nomokonova, T., Maturilli, M., and Ritter, C.: Radiative Effect of Clouds at Ny-Ålesund, Svalbard, as

581 Inferred from Ground-Based Remote Sensing Observations, Journal of Applied Meteorology and Climatology, 59, 3–

582 22, https://doi.org/10.1175/JAMC-D-19-0080.1, 2020.

583 Eirund, G. K., Possner, A., and Lohmann, U.: Response of Arctic mixed-phase clouds to aerosol perturbations under

584 different surface forcings, Atmospheric Chemistry and Physics, 19, 9847–9864, https://doi.org/10.5194/acp-19-9847-

585 2019, 2019.

586 Engvall, A.-C., Krejci, R., Ström, J., Treffeisen, R., Scheele, R., Hermansen, O., and Paatero, J.: Changes in aerosol

587 properties during spring-summer period in the Arctic troposphere, Atmospheric Chemistry and Physics, 8, 445–462,

588 https://doi.org/10.5194/acp-8-445-2008, 2008.

589    Field, P. R., Lawson, R. P., Brown, P. R. A., Lloyd, G., Westbrook, C., Moisseev, D., Miltenberger, A., Nenes, A.,
590    Blyth, A., Choularton, T., Connolly, P., Buehl, J., Crosier, J., Cui, Z., Dearden, C., DeMott, P., Flossmann, A.,
591    Heymsfield, A., Huang, Y., Kalesse, H., Kanji, Z. A., Korolev, A., Kirchgaessner, A., Lasher-Trapp, S., Leisner, T.,
592    McFarquhar, G., Phillips, V., Stith, J., and Sullivan, S.: Secondary Ice Production: Current State of the Science and
593    Recommendations for the Future, Meteorological Monographs, 58, 7.1-7.20,
594    https://doi.org/10.1175/AMSMONOGRAPHS-D-16-0014.1, 2017.

595    Fountoukis, C. and Nenes, A.: Continued development of a cloud droplet formation parameterization for global climate
596    models, Journal of Geophysical Research: Atmospheres, 110, https://doi.org/10.1029/2004JD005591, 2005.

597    Fountoukis, C., Nenes, A., Meskhidze, N., Bahreini, R., Conant, W. C., Jonsson, H., Murphy, S., Sorooshian, A.,
598    Varutbangkul, V., Brechtel, F., Flagan, R. C., and Seinfeld, J. H.: Aerosol–cloud drop concentration closure for clouds
599    sampled during the International Consortium for Atmospheric Research on Transport and Transformation 2004
600    campaign, Journal of Geophysical Research: Atmospheres, 112, https://doi.org/10.1029/2006JD007272, 2007.

601    Freud, E., Krejci, R., Tunved, P., Leaitch, R., Nguyen, Q. T., Massling, A., Skov, H., and Barrie, L.: Pan-Arctic aerosol
602    number size distributions: seasonality and transport patterns, Atmospheric Chemistry and Physics, 17, 8101–8128,
603    https://doi.org/10.5194/acp-17-8101-2017, 2017.

604    Fröhlich, R., Cubison, M. J., Slowik, J. G., Bukowiecki, N., Prévôt, A. S. H., Baltensperger, U., Schneider, J., Kimmel,
605    J. R., Gonin, M., Rohner, U., Worsnop, D. R., and Jayne, J. T.: The ToF-ACSM: a portable aerosol chemical speciation
606    monitor with TOFMS detection, Atmospheric Measurement Techniques, 6, 3225–3241, https://doi.org/10.5194/amt-
607    6-3225-2013, 2013.

608    Garrett, T. J., Zhao, C., Dong, X., Mace, G. G., and Hobbs, P. V.: Effects of varying aerosol regimes on low-level
609    Arctic stratus, Geophysical Research Letters, 31, https://doi.org/10.1029/2004GL019928, 2004.

610    Georgakaki, P., Bougiatioti, A., Wieder, J., Mignani, C., Ramelli, F., Kanji, Z. A., Henneberger, J., Hervo, M., Berne,
611    A., Lohmann, U., and Nenes, A.: On the drivers of droplet variability in alpine mixed-phase clouds, Atmospheric
612    Chemistry and Physics, 21, 10993–11012, https://doi.org/10.5194/acp-21-10993-2021, 2021.

613    Gramlich, Y., Siegel, K., Haslett, S. L., Freitas, G., Krejci, R., Zieger, P., and Mohr, C.: Revealing the chemical
614    characteristics of Arctic low-level cloud residuals &ndash; in situ observations from a mountain site, EGUsphere, 1–
615    29, https://doi.org/10.5194/egusphere-2022-1395, 2022.

616    Graßl, S., Ritter, C., and Schulz, A.: The Nature of the Ny-Ålesund Wind Field Analysed by High-Resolution
617    Windlidar Data, Remote Sensing, 14, 3771, https://doi.org/10.3390/rs14153771, 2022.

618 Gysel, M., Crosier, J., Topping, D. O., Whitehead, J. D., Bower, K. N., Cubison, M. J., Williams, P. I., Flynn, M. J.,
619 Mcfiggans, G. B., and Coe, H.: Closure study between chemical composition and hygroscopic growth of aerosol
620 particles during TORCH2, Atmospheric Chemistry and Physics, 7, 6131–6144, 2007.

621 Hammer, E., Bukowiecki, N., Luo, B. P., Lohmann, U., Marcolli, C., Weingartner, E., Baltensperger, U., and Hoyle,
622 C. R.: Sensitivity estimations for cloud droplet formation in the vicinity of the high-alpine research station Jungfraujoch
623 (3580 m a.s.l.), Atmospheric Chemistry and Physics, 15, 10309–10323, https://doi.org/10.5194/acp-15-10309-2015,
624 2015.

625 Herenz, P., Wex, H., Henning, S., Kristensen, T. B., Rubach, F., Roth, A., Borrmann, S., Bozem, H., Schulz, H., and
626 Stratmann, F.: Measurements of aerosol and CCN properties in the Mackenzie River delta (Canadian Arctic) during
627 spring–summer transition in May 2014, Atmospheric Chemistry and Physics, 18, 4477–4496,
628 https://doi.org/10.5194/acp-18-4477-2018, 2018.

629 Hirdman, D., Burkhart, J. F., Sodemann, H., Eckhardt, S., Jefferson, A., Quinn, P. K., Sharma, S., Ström, J., and Stohl,
630 A.: Long-term trends of black carbon and sulphate aerosol in the Arctic: changes in atmospheric transport and source
631 region emissions, Atmospheric Chemistry and Physics, 10, 9351–9368, https://doi.org/10.5194/acp-10-9351-2010,
632 2010.

633 Hoyle, C. R., Webster, C. S., Rieder, H. E., Nenes, A., Hammer, E., Herrmann, E., Gysel, M., Bukowiecki, N.,
634 Weingartner, E., Steinbacher, M., and Baltensperger, U.: Chemical and physical influences on aerosol activation in
635 liquid clouds: a study based on observations from the Jungfraujoch, Switzerland, Atmospheric Chemistry and Physics,
636 16, 4043–4061, https://doi.org/10.5194/acp-16-4043-2016, 2016.

637 Intrieri, J. M., Fairall, C. W., Shupe, M. D., Persson, P. O. G., Andreas, E. L., Guest, P. S., and Moritz, R. E.: An
638 annual cycle of Arctic surface cloud forcing at SHEBA, Journal of Geophysical Research: Oceans, 107, SHE 13-1-
639 SHE 13-14, https://doi.org/10.1029/2000JC000439, 2002.

640 Jensen, J. B. and Charlson, R. J.: On the efficiency of nucleation scavenging, Tellus B: Chemical and Physical
641 Meteorology, 36, 367–375, https://doi.org/10.3402/tellusb.v36i5.14917, 1984.

642 Jung, C. H., Yoon, Y. J., Kang, H. J., Gim, Y., Lee, B. Y., Ström, J., Krejci, R., and Tunved, P.: The seasonal
643 characteristics of cloud condensation nuclei (CCN) in the arctic lower troposphere, Tellus B: Chemical and Physical
644 Meteorology, 70, 1–13, https://doi.org/10.1080/16000889.2018.1513291, 2018.

645 Kacarab, M., Thornhill, K. L., Dobracki, A., Howell, S. G., O'Brien, J. R., Freitag, S., Poellot, M. R., Wood, R.,
646 Zuidema, P., Redemann, J., and Nenes, A.: Biomass burning aerosol as a modulator of the droplet number in the
647 southeast Atlantic region, Atmospheric Chemistry and Physics, 20, 3029–3040, https://doi.org/10.5194/acp-20-3029-
648 2020, 2020.

649     Kammermann, L., Gysel, M., Weingartner, E., Herich, H., Cziczo, D. J., Holst, T., Svenningsson, B., Arneth, A., and

650     Baltensperger, U.: Subarctic atmospheric aerosol composition: 3. Measured and modeled properties of cloud

651     condensation nuclei, Journal of Geophysical Research: Atmospheres, 115, https://doi.org/10.1029/2009JD012447,

652     2010.

653     Karlsson, L., Krejci, R., Koike, M., Ebell, K., and Zieger, P.: A long-term study of cloud residuals from low-level

654     Arctic clouds, Atmospheric Chemistry and Physics, 21, 8933–8959, https://doi.org/10.5194/acp-21-8933-2021, 2021.

655     Koike, M., Ukita, J., Ström, J., Tunved, P., Shiobara, M., Vitale, V., Lupi, A., Baumgardner, D., Ritter, C., Hermansen,

656     O., Yamada, K., and Pedersen, C. A.: Year-Round In Situ Measurements of Arctic Low-Level Clouds: Microphysical

657     Properties and Their Relationships With Aerosols, Journal of Geophysical Research: Atmospheres, 124, 1798–1822,

658     https://doi.org/10.1029/2018JD029802, 2019.

659     Korolev, A. and Leisner, T.: Review of experimental studies of secondary ice production, Atmospheric Chemistry and

660     Physics, 20, 11767–11797, https://doi.org/10.5194/acp-20-11767-2020, 2020.

661     Korolev, A., McFarquhar, G., Field, P. R., Franklin, C., Lawson, P., Wang, Z., Williams, E., Abel, S. J., Axisa, D.,

662     Borrmann, S., Crosier, J., Fugal, J., Krämer, M., Lohmann, U., Schlenczek, O., Schnaiter, M., and Wendisch, M.:

663     Mixed-Phase Clouds: Progress and Challenges, Meteorological Monographs, 58, 5.1-5.50,

664     https://doi.org/10.1175/AMSMONOGRAPHS-D-17-0001.1, 2017.

665     Lance, S., Shupe, M. D., Feingold, G., Brock, C. A., Cozic, J., Holloway, J. S., Moore, R. H., Nenes, A., Schwarz, J.

666     P., Spackman, J. R., Froyd, K. D., Murphy, D. M., Brioude, J., Cooper, O. R., Stohl, A., and Burkhart, J. F.: Cloud

667     condensation nuclei as a modulator of ice processes in Arctic mixed-phase clouds, Atmospheric Chemistry and Physics,

668     11, 8003–8015, https://doi.org/10.5194/acp-11-8003-2011, 2011.

669     Lathem, T. L., Beyersdorf, A. J., Thornhill, K. L., Winstead, E. L., Cubison, M. J., Hecobian, A., Jimenez, J. L., Weber,

670     R. J., Anderson, B. E., and Nenes, A.: Analysis of CCN activity of Arctic aerosol and Canadian biomass burning during

671     summer 2008, Atmospheric Chemistry and Physics, 13, 2735–2756, https://doi.org/10.5194/acp-13-2735-2013, 2013.

672     Lawson, R. P., Stamnes, K., Stamnes, J., Zmarzly, P., Koskuliks, J., Roden, C., Mo, Q., Carrithers, M., and Bland, G.

673     L.: Deployment of a Tethered-Balloon System for Microphysics and Radiative Measurements in Mixed-Phase Clouds

674     at Ny-Ålesund and South Pole, Journal of Atmospheric and Oceanic Technology, 28, 656–670,

675     https://doi.org/10.1175/2010JTECHA1439.1, 2011.

676     Leaitch, W. R., Korolev, A., Aliabadi, A. A., Burkart, J., Willis, M. D., Abbatt, J. P. D., Bozem, H., Hoor, P., Köllner,

677     F., Schneider, J., Herber, A., Konrad, C., and Brauner, R.: Effects of 20–100 nm particles on liquid clouds in the clean

678     summertime Arctic, Atmospheric Chemistry and Physics, 16, 11107–11124, https://doi.org/10.5194/acp-16-11107-

679     2016, 2016.

680    Liu, Z., Barlow, J. F., Chan, P.-W., Fung, J. C. H., Li, Y., Ren, C., Mak, H. W. L., and Ng, E.: A Review of Progress
681    and Applications of Pulsed Doppler Wind LiDARs, Remote Sensing, 11, 2522, https://doi.org/10.3390/rs11212522,
682    2019.

683    Martin, M., Chang, R. Y.-W., Sierau, B., Sjogren, S., Swietlicki, E., Abbatt, J. P. D., Leck, C., and Lohmann, U.: Cloud
684    condensation nuclei closure study on summer arctic aerosol, Atmospheric Chemistry and Physics, 11, 11335–11350,
685    https://doi.org/10.5194/acp-11-11335-2011, 2011.

686    Massling, A., Lange, R., Pernov, J., Gosewinkel, U., Sørensen, L.-L., and Skov, H.: Measurement report: High Arctic
687    aerosol hygroscopicity at sub- and supersaturated conditions during spring and summer, Atmospheric Chemistry and
688    Physics Discussions, 1–30, https://doi.org/10.5194/acp-2022-413, 2022.

689    Maturilli, M., Herber, A., and König-Langlo, G.: Surface radiation climatology for Ny-Ålesund, Svalbard (78.9° N),
690    basic observations for trend detection, Theor Appl Climatol, 120, 331–339, https://doi.org/10.1007/s00704-014-1173-
691    4, 2015.

692    Maturilli, M., Hanssen-Bauer, I., Neuber, R., Rex, M., and Edvardsen, K.: The Atmosphere Above Ny-Ålesund:
693    Climate and Global Warming, Ozone and Surface UV Radiation, in: The Ecosystem of Kongsfjorden, Svalbard, edited
694    by: Hop, H. and Wiencke, C., Springer International Publishing, Cham, 23–46, https://doi.org/10.1007/978-3-319-
695    46425-1_2, 2019.

696    Mauritsen, T., Sedlar, J., Tjernström, M., Leck, C., Martin, M., Shupe, M., Sjogren, S., Sierau, B., Persson, P. O. G.,
697    Brooks, I. M., and Swietlicki, E.: An Arctic CCN-limited cloud-aerosol regime, Atmospheric Chemistry and Physics,
698    11, 165–173, https://doi.org/10.5194/acp-11-165-2011, 2011.

699    Mioche, G., Jourdan, O., Ceccaldi, M., and Delanoë, J.: Variability of mixed-phase clouds in the Arctic with a focus
700    on the Svalbard region: a study based on spaceborne active remote sensing, Atmospheric Chemistry and Physics, 15,
701    2445–2461, https://doi.org/10.5194/acp-15-2445-2015, 2015.

702    Moore, R. H., Bahreini, R., Brock, C. A., Froyd, K. D., Cozic, J., Holloway, J. S., Middlebrook, A. M., Murphy, D.
703    M., and Nenes, A.: Hygroscopicity and composition of Alaskan Arctic CCN during April 2008, Atmospheric
704    Chemistry and Physics, 11, 11807–11825, https://doi.org/10.5194/acp-11-11807-2011, 2011.

705    Morales Betancourt, R. and Nenes, A.: Droplet activation parameterization: the population-splitting concept revisited,
706    Geoscientific Model Development, 7, 2345–2357, https://doi.org/10.5194/gmd-7-2345-2014, 2014.

707    Najafi, M. R., Zwiers, F. W., and Gillett, N. P.: Attribution of Arctic temperature change to greenhouse-gas and aerosol
708    influences, Nature Clim Change, 5, 246–249, https://doi.org/10.1038/nclimate2524, 2015.

709    Nenes, A. and Seinfeld, J. H.: Parameterization of cloud droplet formation in global climate models, Journal of
710    Geophysical Research: Atmospheres, 108, https://doi.org/10.1029/2002JD002911, 2003.

711     Nenes, A., Ghan, S., Abdul-Razzak, H., Chuang, P. Y., and Seinfeld, J. H.: Kinetic limitations on cloud droplet
712     formation and impact on cloud albedo, Tellus B: Chemical and Physical Meteorology, 53, 133–149,
713     https://doi.org/10.3402/tellusb.v53i2.16569, 2001.

714     Nomokonova, T., Ebell, K., Löhnert, U., Maturilli, M., Ritter, C., and O'Connor, E.: Statistics on clouds and their
715     relation to thermodynamic conditions at Ny-Ålesund using ground-based sensor synergy, Atmospheric Chemistry and
716     Physics, 19, 4105–4126, https://doi.org/10.5194/acp-19-4105-2019, 2019.

717     Norgren, M. S., de Boer, G., and Shupe, M. D.: Observed aerosol suppression of cloud ice in low-level Arctic mixed-
718     phase clouds, Atmospheric Chemistry and Physics, 18, 13345–13361, https://doi.org/10.5194/acp-18-13345-2018,
719     2018.

720     Ohata, S., Mori, T., Kondo, Y., Sharma, S., Hyvärinen, A., Andrews, E., Tunved, P., Asmi, E., Backman, J., Servomaa,
721     H., Veber, D., Eleftheriadis, K., Vratolis, S., Krejci, R., Zieger, P., Koike, M., Kanaya, Y., Yoshida, A., Moteki, N.,
722     Zhao, Y., Tobo, Y., Matsushita, J., and Oshima, N.: Estimates of mass absorption cross sections of black carbon for
723     filter-based absorption photometers in the Arctic, Atmospheric Measurement Techniques, 14, 6723–6748,
724     https://doi.org/10.5194/amt-14-6723-2021, 2021.

725     Park, K.-T., Yoon, Y. J., Lee, K., Tunved, P., Krejci, R., Ström, J., Jang, E., Kang, H. J., Jang, S., Park, J., Lee, B. Y.,
726     Traversi, R., Becagli, S., and Hermansen, O.: Dimethyl Sulfide-Induced Increase in Cloud Condensation Nuclei in the
727     Arctic Atmosphere, Global Biogeochemical Cycles, 35, e2021GB006969, https://doi.org/10.1029/2021GB006969,
728     2021.

729     Pasquier, J. T., Henneberger, J., Ramelli, F., Lauber, A., David, R. O., Wieder, J., Carlsen, T., Gierens, R., Maturilli,
730     M., and Lohmann, U.: Conditions favorable for secondary ice production in Arctic mixed-phase clouds, Atmospheric
731     Chemistry and Physics, 22, 15579–15601, https://doi.org/10.5194/acp-22-15579-2022, 2022a.

732     Pasquier, J. T., David, R. O., Freitas, G., Gierens, R., Gramlich, Y., Haslett, S., Li, G., Schäfer, B., Siegel, K., Wieder,
733     J., Adachi, K., Belosi, F., Carlsen, T., Decesari, S., Ebell, K., Gilardoni, S., Gysel-Beer, M., Henneberger, J., Inoue, J.,
734     Kanji, Z. A., Koike, M., Kondo, Y., Krejci, R., Lohmann, U., Maturilli, M., Mazzolla, M., Modini, R., Mohr, C.,
735     Motos, G., Nenes, A., Nicosia, A., Ohata, S., Paglione, M., Park, S., Pileci, R. E., Ramelli, F., Rinaldi, M., Ritter, C.,
736     Sato, K., Storelvmo, T., Tobo, Y., Traversi, R., Viola, A., and Zieger, P.: The Ny-Ålesund Aerosol Cloud Experiment
737     (NASCENT): Overview and First Results, Bulletin of the American Meteorological Society, 1,
738     https://doi.org/10.1175/BAMS-D-21-0034.1, 2022b.

739     Petters, M. D. and Kreidenweis, S. M.: A single parameter representation of hygroscopic growth and cloud
740     condensation nucleus activity, Atmospheric Chemistry and Physics, 7, 1961–1971, 2007.

741     Platt, S. M., Hov, Ø., Berg, T., Breivik, K., Eckhardt, S., Eleftheriadis, K., Evangeliou, N., Fiebig, M., Fisher, R.,
742     Hansen, G., Hansson, H.-C., Heintzenberg, J., Hermansen, O., Heslin-Rees, D., Holmén, K., Hudson, S., Kallenborn,

743      R., Krejci, R., Krognes, T., Larssen, S., Lowry, D., Lund Myhre, C., Lunder, C., Nisbet, E., Nizzetto, P. B., Park, K.-

744      T., Pedersen, C. A., Aspmo Pfaffhuber, K., Röckmann, T., Schmidbauer, N., Solberg, S., Stohl, A., Ström, J., Svendby,

745      T., Tunved, P., Tørnkvist, K., van der Veen, C., Vratolis, S., Yoon, Y. J., Yttri, K. E., Zieger, P., Aas, W., and Tørseth,

746      K.: Atmospheric composition in the European Arctic and 30 years of the Zeppelin Observatory, Ny-Ålesund,

747      Atmospheric Chemistry and Physics, 22, 3321–3369, https://doi.org/10.5194/acp-22-3321-2022, 2022.

748      Pöhlker, M. L., Zhang, M., Campos Braga, R., Krüger, O. O., Pöschl, U., and Ervens, B.: Aitken mode particles as

749      CCN in aerosol- and updraft-sensitiveregimes of cloud droplet formation, Clouds and Precipitation/Atmospheric

750      Modelling/Troposphere/Physics (physical properties and processes), https://doi.org/10.5194/acp-2021-221, 2021.

751      Rahn, K. A.: Relative importances of North America and Eurasia as sources of arctic aerosol, Atmospheric

752      Environment (1967), 15, 1447–1455, https://doi.org/10.1016/0004-6981(81)90351-6, 1981.

753      Ramelli, F., Beck, A., Henneberger, J., and Lohmann, U.: Using a holographic imager on a tethered balloon system for

754      microphysical observations of boundary layer clouds, Atmospheric Measurement Techniques, 13, 925–939,

755      https://doi.org/10.5194/amt-13-925-2020, 2020.

756      Rantanen, M., Karpechko, A. Y., Lipponen, A., Nordling, K., Hyvärinen, O., Ruosteenoja, K., Vihma, T., and

757      Laaksonen, A.: The Arctic has warmed nearly four times faster than the globe since 1979, Commun Earth Environ, 3,

758      1–10, https://doi.org/10.1038/s43247-022-00498-3, 2022.

759      Rastak, N., Silvergren, S., Zieger, P., Wideqvist, U., Ström, J., Svenningsson, B., Maturilli, M., Tesche, M., Ekman,

760      A. M. L., Tunved, P., and Riipinen, I.: Seasonal variation of aerosol water uptake and its impact on the direct radiative

761      effect at Ny-Ålesund, Svalbard, Atmospheric Chemistry and Physics, 14, 7445–7460, https://doi.org/10.5194/acp-14-

762      7445-2014, 2014.

763      Reutter, P., Su, H., Trentmann, J., Simmel, M., Rose, D., Gunthe, S. S., Wernli, H., Andreae, M. O., and Pöschl, U.:

764      Aerosol- and updraft-limited regimes of cloud droplet formation: influence of particle number, size and hygroscopicity

765      on the activation of cloud condensation nuclei (CCN), Atmospheric Chemistry and Physics, 9, 7067–7080,

766      https://doi.org/10.5194/acp-9-7067-2009, 2009.

767      Seinfeld, J. H., Bretherton, C., Carslaw, K. S., Coe, H., DeMott, P. J., Dunlea, E. J., Feingold, G., Ghan, S., Guenther,

768      A. B., Kahn, R., Kraucunas, I., Kreidenweis, S. M., Molina, M. J., Nenes, A., Penner, J. E., Prather, K. A., Ramanathan,

769      V., Ramaswamy, V., Rasch, P. J., Ravishankara, A. R., Rosenfeld, D., Stephens, G., and Wood, R.: Improving our

770      fundamental understanding of the role of aerosol−cloud interactions in the climate system, Proceedings of the National

771      Academy of Sciences, 113, 5781–5790, https://doi.org/10.1073/pnas.1514043113, 2016.

772      Shupe, M. D. and Intrieri, J. M.: Cloud Radiative Forcing of the Arctic Surface: The Influence of Cloud Properties,

773      Surface Albedo, and Solar Zenith Angle, Journal of Climate, 17, 616–628, https://doi.org/10.1175/1520-

774      0442(2004)017<0616:CRFOTA>2.0.CO;2, 2004.

775  Shupe, M. D., Daniel, J. S., Boer, G. de, Eloranta, E. W., Kollias, P., Long, C. N., Luke, E. P., Turner, D. D., and

776  Verlinde, J.: A Focus On Mixed-Phase Clouds: The Status of Ground-Based Observational Methods, Bulletin of the

777  American Meteorological Society, 89, 1549–1562, https://doi.org/10.1175/2008BAMS2378.1, 2008a.

778  Shupe, M. D., Kollias, P., Persson, P. O. G., and McFarquhar, G. M.: Vertical Motions in Arctic Mixed-Phase

779  Stratiform Clouds, Journal of the Atmospheric Sciences, 65, 1304–1322, https://doi.org/10.1175/2007JAS2479.1,

780  2008b.

781  Siegel, K., Neuberger, A., Karlsson, L., Zieger, P., Mattsson, F., Duplessis, P., Dada, L., Daellenbach, K., Schmale, J.,

782  Baccarini, A., Krejci, R., Svenningsson, B., Chang, R., Ekman, A. M. L., Riipinen, I., and Mohr, C.: Using Novel

783  Molecular-Level Chemical Composition Observations of High Arctic Organic Aerosol for Predictions of Cloud

784  Condensation Nuclei, Environ. Sci. Technol., 56, 13888–13899, https://doi.org/10.1021/acs.est.2c02162, 2022.

785  Sotiropoulou, G., Tjernström, M., Sedlar, J., Achtert, P., Brooks, B. J., Brooks, I. M., Persson, P. O. G., Prytherch, J.,

786  Salisbury, D. J., Shupe, M. D., Johnston, P. E., and Wolfe, D.: Atmospheric Conditions during the Arctic Clouds in

787  Summer Experiment (ACSE): Contrasting Open Water and Sea Ice Surfaces during Melt and Freeze-Up Seasons,

788  Journal of Climate, 29, 8721–8744, https://doi.org/10.1175/JCLI-D-16-0211.1, 2016.

789  Ström, J., Umegård, J., Tørseth, K., Tunved, P., Hansson, H.-C., Holmén, K., Wismann, V., Herber, A., and König-

790  Langlo, G.: One year of particle size distribution and aerosol chemical composition measurements at the Zeppelin

791  Station, Svalbard, March 2000–March 2001, Physics and Chemistry of the Earth, Parts A/B/C, 28, 1181–1190,

792  https://doi.org/10.1016/j.pce.2003.08.058, 2003.

793  Ström, J., Engvall, A. C., Delbart, F., Krejci, R., and Treffeisen, R.: On small particles in the Arctic summer boundary

794  layer: observations at two different heights near Ny-Ålesund, Svalbard, Tellus B: Chemical and Physical Meteorology,

795  61, 473–482, https://doi.org/10.1111/j.1600-0889.2009.00412.x, 2009.

796  Tan, I. and Storelvmo, T.: Evidence of Strong Contributions From Mixed-Phase Clouds to Arctic Climate Change,

797  Geophysical Research Letters, 46, 2894–2902, https://doi.org/10.1029/2018GL081871, 2019.

798  Tjernström, M., Leck, C., Birch, C. E., Bottenheim, J. W., Brooks, B. J., Brooks, I. M., Bäcklin, L., Chang, R. Y.-W.,

799  de Leeuw, G., Di Liberto, L., de la Rosa, S., Granath, E., Graus, M., Hansel, A., Heintzenberg, J., Held, A., Hind, A.,

800  Johnston, P., Knulst, J., Martin, M., Matrai, P. A., Mauritsen, T., Müller, M., Norris, S. J., Orellana, M. V., Orsini, D.

801  A., Paatero, J., Persson, P. O. G., Gao, Q., Rauschenberg, C., Ristovski, Z., Sedlar, J., Shupe, M. D., Sierau, B.,

802  Sirevaag, A., Sjogren, S., Stetzer, O., Swietlicki, E., Szczodrak, M., Vaattovaara, P., Wahlberg, N., Westberg, M., and

803  Wheeler, C. R.: The Arctic Summer Cloud Ocean Study (ASCOS): overview and experimental design, Atmospheric

804  Chemistry and Physics, 14, 2823–2869, https://doi.org/10.5194/acp-14-2823-2014, 2014.

805 Touloupas, G., Lauber, A., Henneberger, J., Beck, A., and Lucchi, A.: A convolutional neural network for classifying
806 cloud particles recorded by imaging probes, Atmospheric Measurement Techniques, 13, 2219–2239,
807 https://doi.org/10.5194/amt-13-2219-2020, 2020.

808 Tunved, P., Ström, J., and Krejci, R.: Arctic aerosol life cycle: linking aerosol size distributions observed between
809 2000 and 2010 with air mass transport and precipitation at Zeppelin station, Ny-Ålesund, Svalbard, Atmospheric
810 Chemistry and Physics, 13, 3643–3660, https://doi.org/10.5194/acp-13-3643-2013, 2013.

811 Turpin, B. J. and Lim, H.-J.: Species Contributions to PM2.5 Mass Concentrations: Revisiting Common Assumptions
812 for Estimating Organic Mass, Aerosol Science and Technology, 35, 602–610,
813 https://doi.org/10.1080/02786820119445, 2001.

814 Twomey, S.: Radiative properties of clouds, Univ of Arizona Press, United States, 1993.

815 Vincent, W. F.: Arctic Climate Change: Local Impacts, Global Consequences, and Policy Implications, in: The
816 Palgrave Handbook of Arctic Policy and Politics, edited by: Coates, K. S. and Holroyd, C., Springer International
817 Publishing, Cham, 507–526, https://doi.org/10.1007/978-3-030-20557-7_31, 2020.

818 von der Weiden, S.-L., Drewnick, F., and Borrmann, S.: Particle Loss Calculator – a new software tool for the
819 assessment of the performance of aerosol inlet systems, Atmospheric Measurement Techniques, 2, 479–494,
820 https://doi.org/10.5194/amt-2-479-2009, 2009.

821 Zábori, J., Rastak, N., Yoon, Y. J., Riipinen, I., and Ström, J.: Size-resolved cloud condensation nuclei concentration
822 measurements in the Arctic: two case studies from the summer of 2008, Atmospheric Chemistry and Physics, 15,
823 13803–13817, https://doi.org/10.5194/acp-15-13803-2015, 2015.

824 Zieger, P., Fierz-Schmidhauser, R., Gysel, M., Ström, J., Henne, S., Yttri, K. E., Baltensperger, U., and Weingartner,
825 E.: Effects of relative humidity on aerosol light scattering in the Arctic, Atmospheric Chemistry and Physics, 10, 3875–
826 3890, https://doi.org/10.5194/acp-10-3875-2010, 2010.

827 Zieger, P., Väisänen, O., Corbin, J. C., Partridge, D. G., Bastelberger, S., Mousavi-Fard, M., Rosati, B., Gysel, M.,
828 Krieger, U. K., Leck, C., Nenes, A., Riipinen, I., Virtanen, A., and Salter, M. E.: Revising the hygroscopicity of
829 inorganic sea salt particles, Nat Commun, 8, 15883, https://doi.org/10.1038/ncomms15883, 2017.

830